Modelling and field measurements in support of the hydrokinetic resource assessment for the Tanana river at Nenana, Alaska

H Toniolo[1*], **P Duvoy**[1], **S Vanlesberg**[2], and **J Johnson**[3]
[1]Department of Civil and Environmental Engineering, University of Alaska Fairbanks, Fairbanks, Alaska, USA
[2]School of Water Resources, University of Littoral, Santa Fe, Argentina
[3]Intitute of Northern Engineering, University of Alaska Fairbanks, Fairbanks, Alaska, USA

The manuscript was received on 8 April 2010 and was accepted after revision for publication on 26 July 2010.

DOI: 10.1243/09576509JPE1017

Abstract: A comprehensive methodology to assess the hydrokinetic potential of a reach of the Tanana river near Nenana, Alaska, is developed to help determine the suitability of the reach for installing and operating hydrokinetic electric turbines. The methodology utilizes field measurements and two-dimensional model simulations to define the discharge, velocity, power density, turbulence, and Froude number throughout the river reach. Thalweg stability is assessed using the maximum cross-sectional velocity, specific discharge, and turbulence. The thalweg was determined to be stable, for the current river condition, from the upstream end of the reach to about 800 m downstream. From 800 m to the end of the reach, at 1100 m, river hydrodynamics indicate an unstable thalweg shifting towards the right bank. The thalweg instability is associated with the transition between upstream and downstream river bends, which may migrate with river stage, bed load, existing bed conditions, and other factors. The flow is subcritical with an average Froude number of 0.30 along the thalweg. Averaged measured velocities along the thalweg are about 1.5 m/s. The average value for instantaneous power density is approximately 4500 W/m^2 at the period of measurement (late August). Study results indicate that hydraulic conditions in the river reach may be suitable for turbine operations above the 800 m location with the exception of a possible eddy located around the 400 m location.

Keywords: stream, resource assessment, numerical modelling, power density, turbulence

1 INTRODUCTION

The need to reduce dependence on fossil fuels and to reduce greenhouse gas emissions is creating an ever-increasing interest in utilizing renewable energy resources, including the kinetic energy from the currents in large rivers using in-stream hydrokinetic power turbines. Alaska, with 40 per cent of the US's hydrokinetic river energy [**1**] and over 300 rural villages located near large rivers that are not connected to a regional electrical grid has a particular interest in taking advantage of in-stream hydrokinetic turbine generation of electrical power [**2**–**4**]. Rural Alaskan communities are particularly affected by energy costs, paying more than three times the US average, a hardship compounded by per capita incomes less than 75 per cent of the US average [**5**]. Energy costs consumed about 10 per cent of the total income in rural villages in 2000 [**6**], and that percentage continues to increase.

Understanding the hydraulic characteristics of a specific reach of river under consideration as a possible location for one or more hydrokinetic turbines is a necessary first step to determine the base-line river dynamics and to plan turbine installations. Since river dynamics respond immediately to objects placed in the current, it is important to know a river's baseline character to assess changes in river dynamics that result from the installation and operation of a turbine.

The suitability of a specific reach of river for the installation and operation of in-stream hydrokinetic turbines (singly or in arrays) depends on river dynamics, bathymetry, and the stability of

*Corresponding author: *Department of Civil and Environmental Engineering, University of Alaska Fairbanks, PO Box 755900, Fairbanks, AK 99775-5900, USA.*
email: hatoniolo@alaska.edu

the high-velocity zones along the channel. The instantaneous power density, specific discharge, and bathymetry as a function of position along the length and width of a river reach determine local power variations, the total practical available power, and the available space for placing turbines. The total recoverable power for a turbine is a function of the total practical available river hydrokinetic power, the effectiveness of a given turbine device at capturing the available energy, and the spacing distance between turbines needed to avoid wake turbulence effects from upstream turbines.

Understanding the characteristics of river turbulence and shear stresses is necessary to estimate the off-directional stresses and stress gradients that may be imposed on a turbine, reducing its efficiency and increasing stress fatigue on turbine structural components. The relative magnitude of river turbulence and shear stresses in a channel can also indicate regions of the channel with net sediment erosion or deposition rates that may signal that the river's thalweg is unstable and migrating. Such migration eventually causes the thalweg to move away from an installed turbine, reducing the percentage of the total available power from the river that can be converted to electricity. Thus, the importance of turbulence in the context of the present work is clear. In this article, the authors focus on turbulence differences in the river channel as a means of assessing channel stability. Detailed analysis of turbulence (i.e. to estimate off-directional stresses and stress gradients) is beyond the scope of this article. In fact, an analysis of this type constitutes a standalone article.

Determining base-line river dynamic characteristics is important as an aid to plan turbine designs, installations, and operations and to evaluate how an installed turbine affects river dynamics. The authors report on an effort to develop a methodology to characterize the hydrodynamics of a reach of the Tanana river, Alaska, to identify the important factors that may affect the design, installation, and operation of a proposed demonstration hydrokinetic turbine installation.

The open water river dynamics during fall (i.e. late August) is the focus of this work. Seasonal variations of the river dynamics during the fall, winter, and spring seasons and sediment transport are the subject of an ongoing study and will be reported at a later date.

2 STUDY SITE AND MOTIVATION

The Ocean Renewable Power Company (ORPC) holds a preliminary Federal Energy Regulatory Commission (FERC) permit to install a hydrokinetic turbine in the reach of the Tanana river near Nenana, Alaska (Fig. 1) located approximately 70 km southwest of Fairbanks, Alaska. The ORPC plans to install a demonstration hydrokinetic turbine in the Tanana at the Nenana location in the 2011–2012 timeframe.

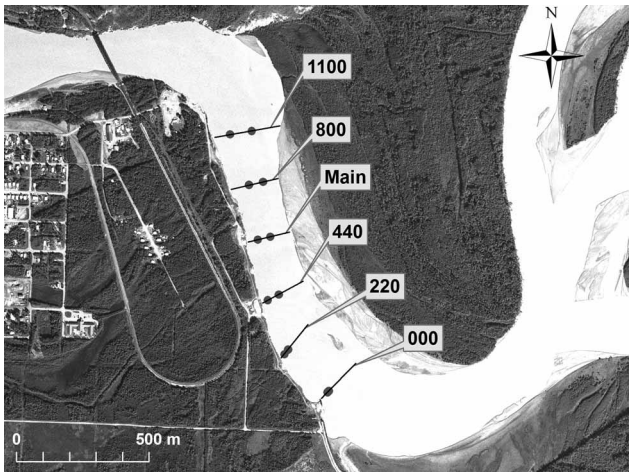

Fig. 1 Aerial view of the study reach. Lines indicate river transects where velocity measurements were made. Flow direction is from right to left

The Tanana river is a large sediment laden glacier-fed river that eventually flows into the Yukon river. River discharge is measured approximately 1.5 km downstream from the reach of the Tanana river which is the focus of this study by the United States Geological Survey (USGS), station ID 15515500. Available data can be found at http://waterdata.usgs.gov/nwis/nwisman/?site_no=15515500. Historical average monthly discharge during the open water season (i.e. May–October) ranges from 495.5 to 1704.7 m^3/s (17 500–60 200 cfs). Winter discharge ranges from 184.6 to 269.9 m^3/s (6520–9530 cfs). Unlike other USGS gauging stations, the Nenana station data are not amenable to relating river discharge to river stage. The Nenana river enters the Tanana just downstream from the gauging station causing variable backwater effects on the Tanana river flow that can affect the river stage separately from the Tanana river discharge, especially during periods of high discharge from the Nenana river.

3 METHODS

The authors' measurement and analysis approach is designed to provide base-line information needed to evaluate several critical factors that can affect, or be affected by, possible hydrokinetic turbine installation and operation that include:

(a) characterizing present river hydrodynamic conditions to be used in evaluating the effects of any future deployed turbines;
(b) determining the current velocity and power density to ensure that turbine operation is technically and economically feasible;

(c) determining the locations within the reach that are suitable for turbine installation by virtue of having a stable thalweg with sufficient current velocity, power density, discharge, and suitable vertical velocity profiles;
(d) determining the riverbed conditions that affect flow and possible turbine installation methods and operations.

3.1 Field work

Field work encompassed a variety of efforts focused on the hydraulic characterization of the Tanana reach. Field tasks involved bathymetric and cross-sectional surveys, and localized velocity measurements at selected points. A description of each effort is given below.

A bathymetric survey was conducted by Terrasond (http://www.terrasond.com/), during August 23–28, 2009. River discharge at the time ranged from 1016.6 to 1141.2 m^3/s (35 900–40 300 cfs). A multibeam echosounder, model ES3 – manufactured by Odom (http://www.odomhydrographic.com/), and a side-scan sonar, model 872 'YellowFin' – manufactured by Imagenix (http://www.imagenex.com/), were used to carry out the hydrographic survey. The bathymetry of the study reach is shown in Fig. 2. As indicated in the figure, the reach is relatively straight, with the channel width expanding in the downstream direction. Minimum and maximum water depths are around 5 and 15 m, at the downstream and upstream end of the study reach, respectively. The average channel width is 155 m, ranging from 90 to 190 m. The river reach is 1260 m long. Also, typical river bed-forms, called dunes, can be identified in the region near the upstream end (Fig. 2).

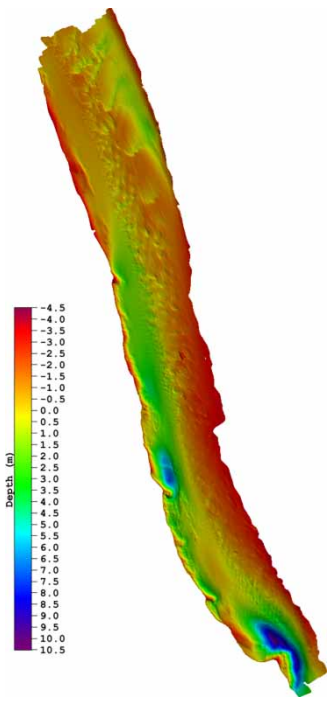

Fig. 2 Bathymetry of the study reach. Flow direction is from bottom to top

In addition to the bathymetric survey, Terrasond conducted six river transects along the reach. An acoustic Doppler current profiler (ADCP), Rio Grande 1200 kHz – manufactured by Teledyne RDI (http://www.rdinstruments.com/), was used to carry out these transects. These ADCP transects are schematically indicated by the labelled lines in Fig. 1. After all transects were performed, two points along each transect were selected to make high-frequency velocity measurements. These velocity measurements were used to calculate river turbulence. The choice of measurement locations was based on the following approach: one point was selected in the deepest point of a given transect (i.e. the thalweg), and the other point coincided with the location of the maximum velocity (outside the thalweg). Thus, the points located in the thalweg and maximum velocity outside of the thalweg were denominated '*thalweg*' and '*maximum*', respectively. Table 1 provides the geographic co-ordinates and depth of each of these locations.

The ADCPs were moored and deployed on the river bottom at each thalweg and maximum point. The ADCPs were configured to collect an ensemble every 0.60 s, with minimal averaging, two pings. Each bin was 0.25 m, with the first bin centred 0.80 m above the transducer head. The transducer head was located 0.27 m above the bottom of the mooring. While the depth of penetration of the mooring into the sediment could not be assessed, it was assumed that the distance was around 0.07 m. This configuration is adequate to perform a study focused on the main characteristics of turbulence in the water column. A similar approach, namely, the use of ADCP at fixed locations to quantify the main turbulence characteristics in a river was reported by Muste *et al.* [**7**]. Data collection time at each point was around 15 min, as suggested by Muste *et al.* [**7**].

Two ADCPs were simultaneously deployed in the thalweg and maximum points along the 1100 transect to investigate the possibility of any temporal correlation between parameters used to estimate turbulence.

3.2 Turbulence and velocity profiles

To estimate main turbulence characteristics, the traditional Reynolds decomposition [**8**] is applied. Reynolds' approach considers each instantaneous velocity component, $\tilde{u}_i$, composed by a mean flow velocity, U_i, and a velocity fluctuation, u_i. In this case, $i = 1 =$ east; $i = 2 =$ north; $i = 3 =$ vertical directions, respectively. Here, vertical is defined positive upwards.

Table 1 Geographic co-ordinates and water depth of selected points along the study reach

Transect		Thalweg		Depth (m)		Maximum		Depth (m)
000	Latitude	64°	33.359 640′ N	13.6	Latitude	64°	33.362 280′ N	12.2
	Longitude	149°	3.610 510′ W		Longitude	149°	3.604 210′ W	
220	Latitude	64°	33.433 860′ N	6.7	Latitude	64°	33.443 870′ N	5.6
	Longitude	149°	3.819 790′ W		Longitude	149°	3.804 300′ W	
440	Latitude	64°	33.543 040′ N	10.9	Latitude	64°	33.554 730′ N	4.8
	Longitude	149°	3.906 080′ W		Longitude	149°	3.856 700′ W	
Main	Latitude	64°	33.664 920′ N	7.4	Latitude	64°	33.671 140′ N	4.5
	Longitude	149°	3.963 320′ W		Longitude	149°	3.904 190′ W	
800	Latitude	64°	33.775 330′ N	6.4	Latitude	64°	33.782 230′ N	4.3
	Longitude	149°	4.014 080′ W		Longitude	149°	3.948 360′ W	
1100	Latitude	64°	33.885 000′ N	7.2	Latitude	64°	33.876 490′ N	4.4
	Longitude	149°	4.009 030′ W		Longitude	149°	4.110 310′ W	

Then, each velocity component can be expressed as

$$\tilde{u}_i = U_i + u_i \tag{1}$$

To estimate the velocity fluctuations in the i direction, the mean velocity in the i direction is calculated from the available dataset. Then, equation (1) is rearranged to calculate each velocity fluctuation. The averages of the products of velocity fluctuations in two (shear) directions (i.e. $\overline{u_1 u_2}$, east*north; $\overline{u_1 u_3}$, east*vertical; $\overline{u_2 u_3}$, north*vertical) and the average of the squared velocity fluctuations in each normal direction (i.e. $\overline{u_i^2}$; east*east, north*north, vertical*vertical) multiplied by the fluid density represent the Reynolds shear and normal stresses within the flow and are the basic parameters of turbulence [**8**, **9**]. Since the water fluid density is a constant, the relative magnitudes of the Reynolds stresses are described by the average of the tensor products of the velocity fluctuations given by

$$R_{ij} = \rho \overline{u_i u_j} \tag{2}$$

where R_{ij} is the Reynolds stress. This methodology was applied to each bin along the water column in all transects (i.e. 000, 220, 440, Main, 800, and 1100).

A linear regression analysis [**10**, **11**] was applied to the velocity fluctuations in maximum and thalweg in transect 1100, where velocity measurements were collected simultaneously. The purpose of this analysis was to provide insights on the validity of the comparison between turbulent shear stresses discussed in the subsequent paragraphs. Given the fact that the water depths were different (7.2 m in thalweg, and 4.4 m in maximum), two approaches were considered:

(a) compare cells located at the same distance from the bottom, moving upward;
(b) compare cells located at the same depth from the water surface, moving down.

Results from both approaches indicated no correlation between velocity fluctuations in different bins located in thalweg and maximum. Then, one can conclude that any analysis on turbulence can be done on measurements that were not taken simultaneously.

3.3 Numerical work

An existing numerical model, the CCHE2D, developed by researchers at the National Center for Computational Hydroscience and Engineering (NCCHE), University of Mississippi (http://www.ncche.olemiss.

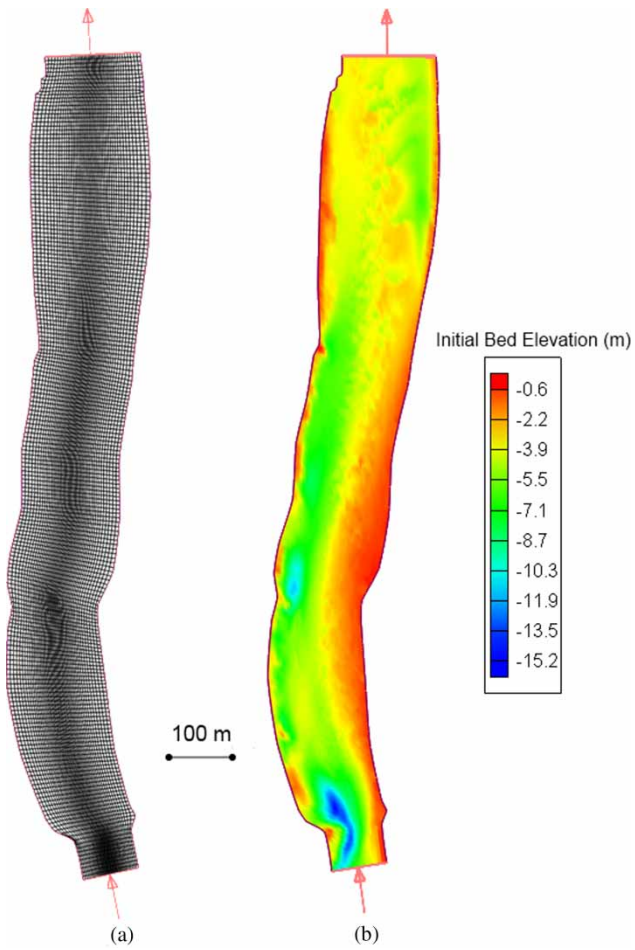

Fig. 3 (a) Computational mesh used in the numerical model and (b) Bathymetry reproduced by the model

edu/), was used in the present work. The model is free, but is not open source. Thus, the model can be exploited but no changes can be made to it. Recently, the software developers expanded the CCHE2D model to a fully three-dimensional (3D) model [**12**]. However, this model is not available for public use yet. The CCHE2D model package is composed of two different applications, CCHE_GUI, the 2D flow and sediment transport model, and CCHE_MESH, the mesh generator.

The CCHE2D is a depth-integrated 2D model for studying steady/unsteady, turbulent flows in open channels with irregular cross-sections, topography, and bank protection structures. The model is capable of simulating bed evolution (i.e. aggradation and erosion) [**13**]. Extensive verification and validation tests were performed to ensure that the numerical model and software implementation are capable of reproducing realistic flow parameters in streams. For instance, the model was used to simulate flow conditions in different settings such as the river Neckar, Germany, the East Fork river of Wyoming, USA. The interaction between flow and training hydraulic structures was adequately simulated at multiple locations along the Mississippi river in Louisiana. Multiple dikes along the Wanan river, downstream from the Wanan reservoir, China were also successfully simulated by the model [**14**].

Table 2 Velocity characteristics – transect 000 – thalweg

Distance from bed (m)	Velocity components (m/s)			Velocity magnitude (m/s)	Average of velocity fluctuations $(m/s)^2$					
	East	North	Vertical		$\overline{u_1^2}$	$\overline{u_2^2}$	$\overline{u_3^2}$	$\overline{u_1 u_2}$	$\overline{u_1 u_3}$	$\overline{u_2 u_3}$
1.00	−0.812	0.838	−0.041	1.168	0.147	0.136	0.031	0.000	0.017	0.006
1.25	−0.830	0.875	−0.067	1.208	0.167	0.148	0.035	−0.003	0.018	0.006
1.50	−0.844	0.917	−0.089	1.250	0.196	0.172	0.038	0.004	0.024	0.009
1.75	−0.872	0.957	−0.111	1.300	0.212	0.183	0.040	0.013	0.028	0.010
2.00	−0.896	0.991	−0.132	1.342	0.233	0.196	0.042	0.021	0.031	0.013
2.25	−0.900	1.044	−0.149	1.386	0.252	0.201	0.042	0.025	0.036	0.014
2.50	−0.926	1.074	−0.164	1.428	0.266	0.204	0.040	0.025	0.036	0.015
2.75	−0.953	1.102	−0.180	1.469	0.270	0.211	0.039	0.026	0.036	0.019
3.00	−0.972	1.133	−0.193	1.505	0.276	0.215	0.038	0.022	0.035	0.022
3.25	−0.992	1.162	−0.204	1.541	0.278	0.216	0.036	0.025	0.034	0.023
3.50	−1.006	1.195	−0.212	1.576	0.268	0.206	0.033	0.022	0.031	0.023
3.75	−1.032	1.237	−0.220	1.626	0.254	0.203	0.032	0.023	0.030	0.026
4.00	−1.057	1.268	−0.230	1.667	0.239	0.195	0.030	0.020	0.026	0.027
4.25	−1.070	1.285	−0.236	1.688	0.221	0.195	0.028	0.018	0.024	0.028
4.50	−1.083	1.316	−0.241	1.722	0.211	0.183	0.027	0.020	0.024	0.028
4.75	−1.099	1.340	−0.245	1.750	0.197	0.180	0.025	0.019	0.021	0.027
5.00	−1.114	1.361	−0.247	1.776	0.185	0.175	0.024	0.018	0.019	0.026
5.25	−1.127	1.378	−0.248	1.797	0.173	0.163	0.022	0.019	0.017	0.025
5.50	−1.132	1.388	−0.248	1.808	0.159	0.161	0.020	0.021	0.015	0.024
5.75	−1.149	1.402	−0.247	1.829	0.149	0.156	0.018	0.017	0.012	0.022
6.00	−1.160	1.419	−0.246	1.849	0.137	0.159	0.017	0.017	0.010	0.022
6.25	−1.169	1.431	−0.245	1.864	0.125	0.151	0.015	0.019	0.009	0.019
6.50	−1.181	1.440	−0.242	1.878	0.121	0.149	0.015	0.019	0.009	0.020
6.75	−1.195	1.446	−0.239	1.891	0.111	0.139	0.014	0.015	0.008	0.019
7.00	−1.208	1.450	−0.235	1.902	0.107	0.136	0.013	0.016	0.007	0.019
7.25	−1.211	1.451	−0.231	1.904	0.100	0.135	0.012	0.018	0.007	0.019
7.50	−1.221	1.454	−0.226	1.912	0.096	0.128	0.012	0.016	0.006	0.018
7.75	−1.226	1.457	−0.221	1.917	0.092	0.128	0.011	0.015	0.006	0.018
8.00	−1.235	1.452	−0.217	1.918	0.089	0.130	0.011	0.017	0.005	0.018
8.25	−1.237	1.453	−0.210	1.920	0.087	0.125	0.010	0.017	0.005	0.017
8.50	−1.251	1.451	−0.204	1.927	0.086	0.118	0.010	0.019	0.005	0.015
8.75	−1.258	1.446	−0.198	1.927	0.085	0.118	0.010	0.022	0.005	0.015
9.00	−1.267	1.440	−0.191	1.927	0.082	0.119	0.009	0.021	0.004	0.015
9.25	−1.278	1.429	−0.186	1.927	0.080	0.120	0.008	0.024	0.004	0.015
9.50	−1.279	1.427	−0.177	1.924	0.073	0.115	0.008	0.024	0.004	0.013
9.75	−1.281	1.425	−0.171	1.924	0.072	0.111	0.007	0.021	0.003	0.013
10.00	−1.293	1.419	−0.165	1.927	0.071	0.105	0.007	0.023	0.004	0.012
10.25	−1.303	1.413	−0.157	1.929	0.065	0.105	0.007	0.023	0.004	0.012
10.50	−1.306	1.407	−0.150	1.926	0.063	0.102	0.006	0.024	0.004	0.012
10.75	−1.314	1.406	−0.143	1.929	0.061	0.096	0.006	0.024	0.003	0.011
11.00	−1.318	1.396	−0.133	1.925	0.056	0.090	0.006	0.021	0.003	0.010
11.25	−1.324	1.397	−0.123	1.929	0.057	0.089	0.006	0.020	0.003	0.010
11.50	−1.337	1.374	−0.116	1.920	0.053	0.082	0.005	0.015	0.002	0.009
11.75	−1.343	1.360	−0.110	1.915	0.051	0.077	0.005	0.015	0.002	0.009
12.00	−1.352	1.350	−0.103	1.914	0.049	0.074	0.005	0.014	0.002	0.009
12.25	−1.362	1.340	−0.094	1.913	0.047	0.068	0.005	0.015	0.002	0.008
12.50	−1.373	1.325	−0.086	1.910	0.046	0.066	0.004	0.014	0.003	0.008
12.75	−1.400	1.289	−0.079	1.905	0.049	0.072	0.004	0.019	0.003	0.008
13.00	−1.391	1.310	−0.069	1.912	0.045	0.062	0.004	0.014	0.002	0.007
13.25	−1.406	1.299	−0.062	1.915	0.042	0.059	0.004	0.011	0.003	0.006

The CCHE2D numerical model is based on a mixed finite-element and finite-volume method to solve the continuity equation on a staggered grid and the momentum equations on a collocated grid. This partially staggered arrangement prevents oscillation caused by a collocated grid where the velocity and pressure fields are decoupled [**15**].

The model simultaneously solves the continuity and momentum equations. It is also capable of accounting for the rotation of water bodies by using a Coriolis parameter. Reynolds stresses in the momentum equations are approximated based on the Boussinesq's assumptions. Closure relations are based on a depth-integrated parabolic model or a 2D ε-k model. Sediment transport equations accounting for suspended and bed loads, as well as an equation to track the bed evolution, complete the model's main equations. For additional details about the main equations and the numerical schemes used to solve them, the reader is directed to the model user manuals [**13**].

3.3.1 *Model implementation*

The steps involved in the model implementation include:

(a) mesh generation;
(b) specification of boundary conditions;
(c) parameter setting.

3.3.2 *Mesh generation*

The mesh represents the computational domain where the governing equations are discretized. It is generated by the CCHE_MESH software, which is also available at NCCHE website. Figures 3(a) and (b) show the mesh built to simulate the study site (i.e. the

Table 3 Velocity characteristics – transect 000 – maximum

Distance from bed (m)	Velocity components (m/s)			Velocity magnitude (m/s)	Average of velocity fluctuations $(m/s)^2$					
	East	North	Vertical		$\overline{u_1^2}$	$\overline{u_2^2}$	$\overline{u_3^2}$	$\overline{u_1u_2}$	$\overline{u_1u_3}$	$\overline{u_2u_3}$
1.00	−0.348	1.285	0.264	1.357	0.063	0.094	0.011	0.004	0.011	0.013
1.25	−0.391	1.363	0.284	1.446	0.063	0.087	0.012	0.005	0.011	0.011
1.50	−0.414	1.408	0.291	1.496	0.061	0.085	0.013	0.000	0.010	0.010
1.75	−0.434	1.428	0.293	1.521	0.059	0.084	0.014	0.002	0.010	0.011
2.00	−0.458	1.445	0.294	1.544	0.062	0.085	0.015	0.003	0.010	0.013
2.25	−0.485	1.451	0.294	1.558	0.065	0.088	0.016	0.011	0.012	0.014
2.50	−0.497	1.461	0.294	1.571	0.069	0.090	0.018	0.009	0.013	0.015
2.75	−0.511	1.474	0.295	1.588	0.075	0.097	0.019	0.006	0.014	0.017
3.00	−0.524	1.467	0.295	1.585	0.079	0.104	0.021	0.007	0.015	0.019
3.25	−0.546	1.460	0.292	1.586	0.081	0.113	0.022	0.010	0.017	0.022
3.50	−0.567	1.447	0.286	1.580	0.089	0.121	0.025	0.009	0.019	0.025
3.75	−0.593	1.431	0.278	1.574	0.092	0.123	0.025	0.010	0.020	0.025
4.00	−0.610	1.425	0.278	1.575	0.094	0.129	0.025	0.012	0.019	0.026
4.25	−0.631	1.402	0.271	1.561	0.103	0.137	0.027	0.017	0.023	0.029
4.50	−0.679	1.375	0.261	1.555	0.107	0.138	0.028	0.019	0.025	0.030
4.75	−0.707	1.352	0.251	1.546	0.112	0.137	0.029	0.023	0.027	0.031
5.00	−0.742	1.326	0.239	1.538	0.117	0.139	0.029	0.023	0.027	0.032
5.25	−0.779	1.301	0.226	1.533	0.116	0.140	0.029	0.024	0.028	0.032
5.50	−0.812	1.278	0.216	1.530	0.113	0.140	0.028	0.026	0.027	0.034
5.75	−0.845	1.250	0.204	1.523	0.110	0.139	0.028	0.029	0.027	0.035
6.00	−0.879	1.220	0.191	1.516	0.113	0.141	0.028	0.030	0.027	0.036
6.25	−0.917	1.183	0.178	1.507	0.111	0.142	0.027	0.030	0.027	0.035
6.50	−0.964	1.135	0.163	1.498	0.108	0.143	0.027	0.030	0.028	0.037
6.75	−0.998	1.101	0.152	1.493	0.107	0.140	0.026	0.029	0.027	0.036
7.00	−1.023	1.069	0.140	1.486	0.103	0.131	0.025	0.028	0.026	0.035
7.25	−1.056	1.037	0.129	1.486	0.101	0.129	0.025	0.024	0.025	0.034
7.50	−1.082	1.003	0.117	1.480	0.098	0.127	0.023	0.019	0.023	0.032
7.75	−1.112	0.968	0.103	1.477	0.092	0.119	0.022	0.014	0.020	0.030
8.00	−1.140	0.939	0.091	1.480	0.093	0.117	0.019	0.013	0.020	0.028
8.25	−1.171	0.911	0.079	1.486	0.083	0.107	0.017	0.009	0.017	0.025
8.50	−1.202	0.891	0.069	1.497	0.078	0.099	0.015	0.002	0.014	0.022
8.75	−1.259	0.867	0.058	1.530	0.070	0.089	0.013	−0.001	0.012	0.020
9.00	−1.295	0.857	0.049	1.554	0.064	0.080	0.012	−0.004	0.010	0.017
9.25	−1.317	0.842	0.042	1.564	0.065	0.075	0.010	0.002	0.010	0.016
9.50	−1.330	0.817	0.043	1.562	0.062	0.061	0.010	−0.004	0.010	0.013
9.75	−1.370	0.800	0.035	1.586	0.058	0.054	0.008	0.001	0.009	0.011
10.00	−1.401	0.787	0.027	1.607	0.046	0.045	0.006	−0.002	0.007	0.008
10.25	−1.426	0.735	0.007	1.604	0.038	0.046	0.007	−0.004	0.004	0.011
10.50	−1.448	0.721	0.001	1.618	0.033	0.042	0.005	−0.006	0.002	0.010
10.75	−1.411	0.736	0.029	1.592	0.034	0.036	0.004	−0.005	0.002	0.007
11.00	−1.526	0.715	0.015	1.685	0.017	0.022	0.001	−0.002	0.001	0.002
11.25	−1.541	0.699	0.002	1.692	0.031	0.032	0.004	0.002	0.005	0.006
11.50	−1.533	0.692	−0.001	1.682	0.032	0.035	0.004	−0.002	0.003	0.006
11.75	−1.527	0.685	−0.008	1.674	0.041	0.044	0.005	−0.004	0.003	0.008
12.00	−1.515	0.674	−0.014	1.658	0.047	0.054	0.006	−0.007	0.003	0.011

Tanana river at Nenana) and the bathymetry generated by the model, respectively. The mesh consists of 200 by 48 lines, resulting in a total of 9600 nodes. Line separation, spacing, and orientation are critical elements of a successful mesh. Additional mesh configurations (i.e. more nodes) were tested before exploiting the code. It was found that results attained with 9600 nodes were similar to other results obtained with a more refined mesh. Thus, the computational time required to run the model was substantially reduced.

3.3.3 *Boundary conditions*

The CCHE2D requires inlet and outlet boundary conditions. Here, the upstream boundary condition was provided in terms of a total steady discharge, Q, set to 1141.2 m^3/s (40 300 cfs). The downstream boundary condition was set in terms of the water surface level, defined here as 0 m (datum). The selected boundary conditions correspond to the river characteristics at the time of conducting the field work.

3.3.4 *Parameter setting*

Input parameters required by the model include: initial water surface elevation for the entire domain, which was set at 0 m; total simulation period; and time step increments. The total simulation period was set to 5000 s. Several trials were made before setting the time step equal to 1 s. Friction factor, Manning's n, was set to 0.03, which coincides with bed sediments found in the study reach. A parabolic eddy viscosity model was used to close the momentum equations.

Table 4 Velocity characteristics – transect 1100 – thalweg

Distance from bed (m)	Velocity components (m/s)			Velocity magnitude (m/s)	Average of velocity fluctuations $(m/s)^2$					
	East	North	Vertical		$\overline{u_1^2}$	$\overline{u_2^2}$	$\overline{u_3^2}$	$\overline{u_1u_2}$	$\overline{u_1u_3}$	$\overline{u_2u_3}$
1.00	−0.372	1.508	−0.042	1.553	0.021	0.024	0.002	−0.001	−0.001	−0.002
1.25	−0.386	1.563	−0.030	1.611	0.022	0.025	0.002	0.000	−0.001	−0.002
1.50	−0.405	1.611	−0.018	1.661	0.020	0.025	0.002	0.000	−0.001	−0.002
1.75	−0.411	1.661	−0.014	1.711	0.020	0.026	0.001	−0.001	−0.001	−0.002
2.00	−0.416	1.704	−0.013	1.754	0.021	0.023	0.001	−0.001	−0.001	−0.002
2.25	−0.420	1.735	−0.010	1.785	0.018	0.023	0.001	0.000	−0.001	−0.002
2.50	−0.424	1.770	−0.010	1.820	0.018	0.021	0.001	−0.001	0.000	−0.001
2.75	−0.427	1.805	−0.010	1.854	0.016	0.019	0.001	0.000	−0.001	−0.001
3.00	−0.424	1.836	−0.009	1.884	0.015	0.017	0.001	0.000	0.000	−0.001
3.25	−0.432	1.860	−0.008	1.909	0.015	0.016	0.001	0.000	0.000	−0.001
3.50	−0.433	1.882	−0.007	1.932	0.015	0.015	0.001	−0.001	−0.001	−0.001
3.75	−0.435	1.904	−0.004	1.953	0.015	0.015	0.001	−0.001	−0.001	−0.001
4.00	−0.439	1.924	−0.003	1.973	0.014	0.016	0.001	0.000	0.000	−0.001
4.25	−0.433	1.893	−0.001	1.942	0.017	0.026	0.002	0.000	0.000	−0.001
4.50	−0.348	1.745	0.033	1.780	0.030	0.026	0.002	0.000	0.001	0.000
4.75	−0.380	1.847	0.012	1.886	0.021	0.035	0.002	−0.004	−0.001	−0.003
5.00	−0.423	1.893	0.007	1.940	0.028	0.031	0.002	−0.001	−0.001	−0.001
5.25	−0.419	1.872	0.010	1.919	0.026	0.031	0.002	0.001	−0.001	−0.001
5.50	−0.424	1.853	0.014	1.901	0.027	0.030	0.002	−0.001	−0.001	−0.001
5.75	−0.423	1.819	0.016	1.868	0.025	0.031	0.002	−0.001	−0.001	−0.001
6.00	−0.414	1.799	0.018	1.846	0.026	0.031	0.002	−0.001	−0.001	−0.001
6.25	−0.409	1.761	0.021	1.808	0.025	0.031	0.002	−0.001	−0.001	−0.001
6.50	−0.409	1.732	0.021	1.780	0.025	0.031	0.002	−0.001	−0.001	−0.001
6.75	−0.408	1.706	0.022	1.754	0.025	0.029	0.002	−0.001	−0.001	0.000
7.00	−0.401	1.683	0.022	1.731	0.025	0.029	0.002	−0.001	−0.001	0.000

Table 5 Velocity characteristics – transect 1100 – maximum

Distance from bed (m)	Velocity components (m/s)			Velocity magnitude (m/s)	Average of velocity fluctuations $(m/s)^2$					
	East	North	Vertical		$\overline{u_1^2}$	$\overline{u_2^2}$	$\overline{u_3^2}$	$\overline{u_1u_2}$	$\overline{u_1u_3}$	$\overline{u_2u_3}$
1.00	−0.508	1.302	−0.050	1.398	0.037	0.039	0.003	0.001	−0.001	0.002
1.25	−0.530	1.351	−0.041	1.452	0.031	0.035	0.003	0.001	−0.001	0.002
1.50	−0.542	1.393	−0.025	1.495	0.033	0.034	0.003	0.002	−0.001	0.002
1.75	−0.555	1.420	−0.022	1.524	0.031	0.035	0.003	0.001	−0.001	0.002
2.00	−0.571	1.457	−0.018	1.565	0.030	0.034	0.003	0.001	−0.001	0.002
2.25	−0.579	1.488	−0.017	1.597	0.027	0.032	0.002	0.001	−0.001	0.002
2.50	−0.582	1.537	−0.016	1.643	0.026	0.027	0.002	0.000	−0.001	0.003
2.75	−0.593	1.555	−0.018	1.664	0.025	0.024	0.002	0.000	−0.001	0.002
3.00	−0.606	1.586	−0.016	1.698	0.019	0.022	0.002	0.000	−0.001	0.003
3.25	−0.604	1.595	−0.017	1.705	0.019	0.021	0.002	0.001	−0.001	0.003
3.50	−0.608	1.603	−0.017	1.715	0.017	0.019	0.002	−0.001	−0.001	0.003
3.75	−0.604	1.612	−0.014	1.721	0.016	0.018	0.002	0.000	−0.001	0.003
4.00	−0.620	1.615	−0.007	1.730	0.016	0.016	0.002	−0.001	−0.001	0.003
4.25	−0.564	1.552	−0.008	1.652	0.016	0.016	0.001	−0.002	−0.001	0.002

4 RESULTS AND DISCUSSION

4.1 Turbulence and velocity profiles

The profiles of velocity fluctuations, $\overline{u_i^2}$, and the shear products of the velocity fluctuations ($\overline{u_1 u_2}$, $\overline{u_1 u_3}$, $\overline{u_2 u_3}$) used in the turbulence analysis are given in Tables 2 to 5. The $\overline{u_i^2}$, for thalweg and maximum for transects 000 and 1100 shown in Figs 4 and 5 and Tables 2 to 5 represent the relative difference in turbulence magnitude between the two locations. The profiles of $\overline{u_i^2}$ are directly proportional to the fluid normal stresses, which are the turbulence parameters. Available data for other transects can be

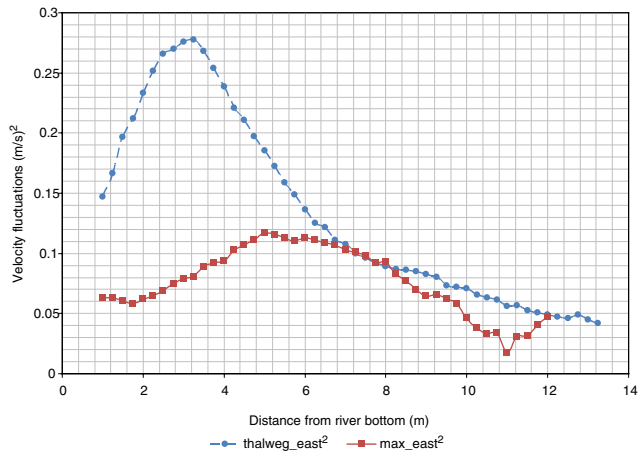

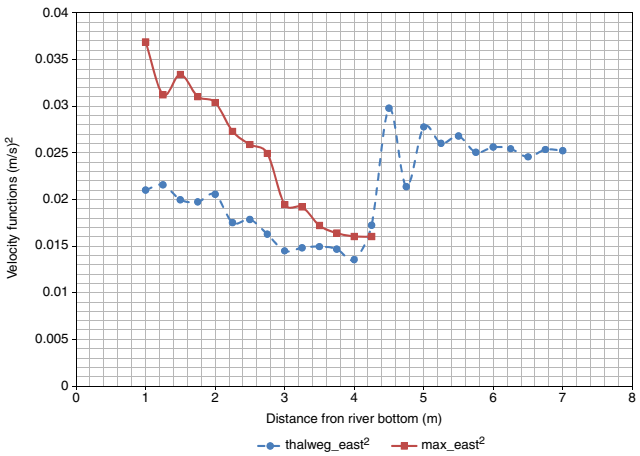

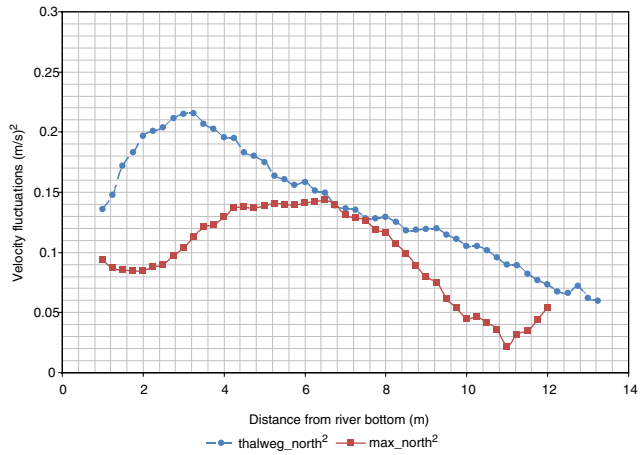

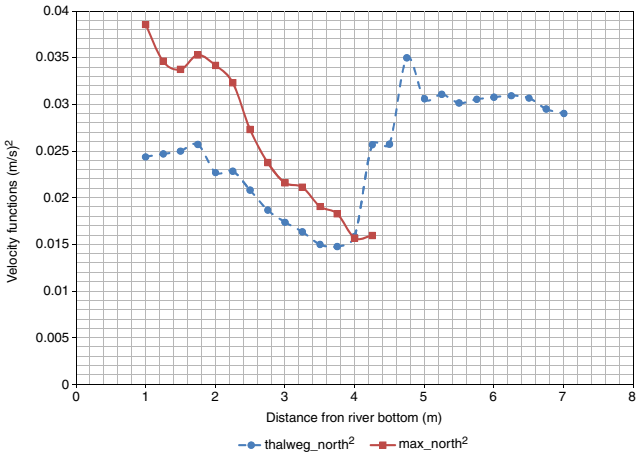

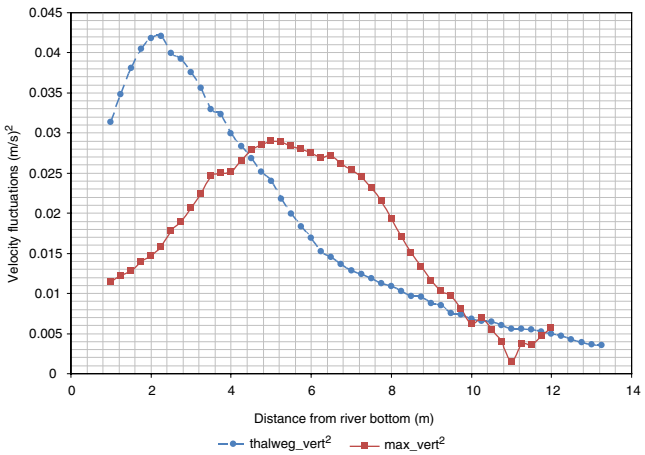

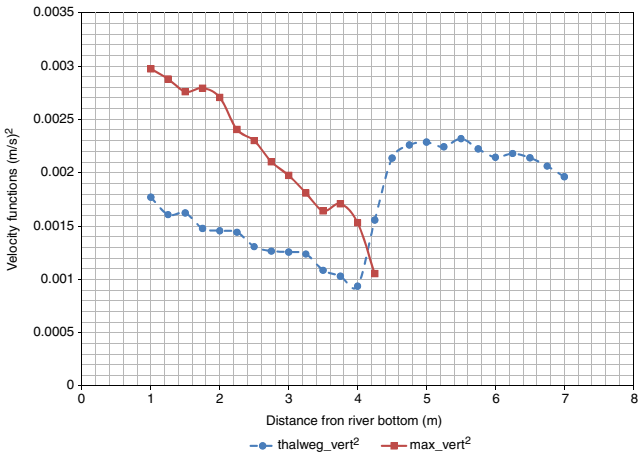

Fig. 4 Transect 000 – comparison between average of velocity fluctuations squared, which are proportional to normal stresses in *thalweg* and *maximum* locations

Fig. 5 Transect 1100 – comparison between average of velocity fluctuations squared, which are proportional to normal stresses in *thalweg* and *maximum* locations

found at http://www.uaf.edu/acep/facilities/alaska-hydrokinetic-energ/tanana_turbulence/. A comparison of the $\overline{u_i^2}$ for thalweg and maximum (Figs 4 and 5) and the turbulence data given in Tables 2 to 5 (along with the online data) indicate that turbulence, in general, is higher in thalweg than in maximum for all transects except transect 1100. Available data for transect 1100 (Table 5 and Fig. 5) indicate that higher turbulence parameters near the riverbed are localized in maximum. A sudden increase in turbulence at 4 m above the riverbed at 1100 thalweg indicates the presence of a strong shear layer associated with a shift of the maximum specific discharge towards the right bank. Thus, the results indicate that the thalweg might be stable from the upstream end to approximately the 800 transect, and unstable from that point to the downstream end. This interpretation of measurements agrees with conclusions reached in modelling described in the following section.

The moored ADCP velocity data were used to calculate relative velocity magnitudes as a function of relative position on a vertical velocity profile at each bin along the water column for the maximum (Fig. 6) and the thalweg locations (Fig. 7) for all transects. The relative velocity, shown in the horizontal axis in Figs 6 and 7, is scaled by the maximum velocity in the given vertical velocity profile; the vertical axis represents the bin's relative position with respect to the water depth. This approach is commonly used in studies related to boundary layers [**16**] and flume studies conducted in a laboratory [**17**, **18**]. Thus, the profiles in the figures give an indication of the similarity condition of velocity profiles along the study reach, which in turn provides an indirect characterization of the river hydrodynamics.

The results shown in Fig. 6 indicate that the flow in maximum is somewhat similar along the study reach, with the exception of the profile located at the

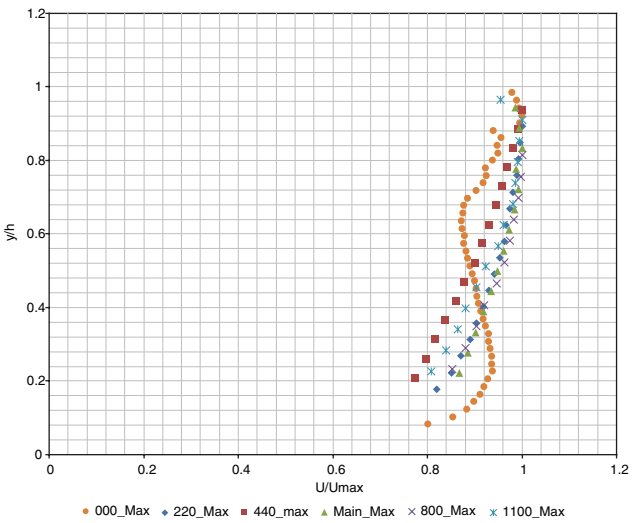

Fig. 6 Dimensionless velocity profiles in *maximum* locations

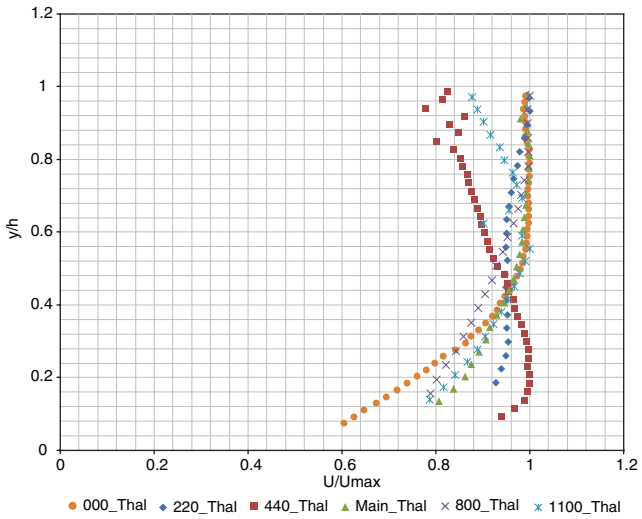

Fig. 7 Dimensionless velocity profiles in *thalweg* locations

upstream end (i.e. transect 000) of the reach that is located immediately downstream of a river bend. Data in Fig. 7 indicate that the flow condition in thalweg does not have a common, similar, velocity profile for any of the transects. In other words, the hydrodynamic condition along the thalweg is highly variable along the reach. The lack of similarity along the thalweg imposes an additional uncertainty in the selection of specific sites to deploy the hydrokinetic device in the study reach.

At this point, it is important to mention that flow condition along a river reach that contains two consecutive and opposite bends creates a pattern similar to the one schematized in Fig. 8. The thalweg is located near the left bank upstream and close to the right bank downstream. This situation is in agreement with the morphologic characteristics found in the study area and its surroundings. The second river bend is located downstream of the study reach. Thus, the thalweg needs to shift from one bank to the other bank along

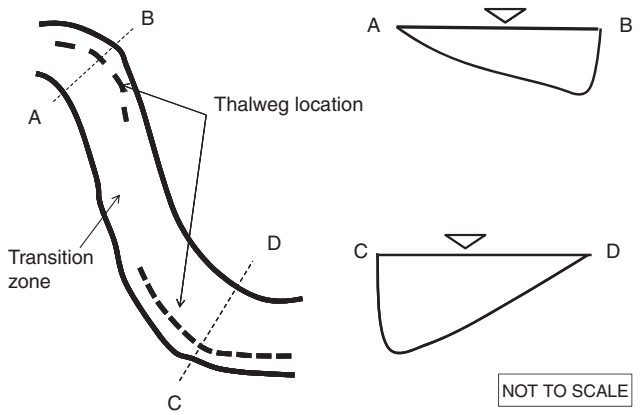

Fig. 8 Schematic view of cross-sections and thalweg location between two consecutives river bends. Flow direction is from right to left

the reach that connects both curves. The specific location where the thalweg shifts is a function of multiple factors, such as river stage, pre-existing bed configuration, sediment load, etc. It should be noticed that the shift rate will evolve with time.

The authors speculate that some peculiarities shown in the data, such as the sudden change in turbulence levels in transect 1100 – thalweg (Fig. 5), the localized reduction in velocity at point $y/h = 0.62$ for the same transect and location (Fig. 7), or the relative high turbulence in maximum compared to thalweg in transect 1100 are strictly related to flow instabilities associated with thalweg displacement in that area.

4.2 Model results

Model results are first discussed as they relate to the river hydraulics and then are analysed from a hydrokinetic point of view; specifically, calculating the instantaneous power density of a parcel of fluid over the river reach.

Velocity and specific discharge distributions generated by the model are shown in Figs 9(a) and 10(a). The high velocities and high specific discharges shown in the figures, in general, agree with the bathymetry, such that high velocities are located in deep areas. This situation is true in approximately 80 per cent of the model domain of the river reach. Some discrepancies appear near the downstream end, where high velocities are located near the left bank, but high specific discharges are located close to the centre of the river or towards the right bank. Thus, the results indicate that the thalweg might be stable from the upstream end of the river reach to approximately the 800 transect, and unstable from that point to the downstream end. Turbulence and velocity measurements are consistent with the model results such that at transect 1100 turbulence magnitudes near the riverbed are greater in maximum than in thalweg. In addition, a strong flow shear occurs at 4 m above the riverbed, as indicated by the sudden increase in turbulence (Fig. 5) and velocity discontinuity (Fig. 7) as the maximum specific discharge shifts from the left bank to the right bank (Fig. 10(b)). Furthermore, the discharge above the shear layer becomes less concentrated (Fig. 10(a)) resulting in a reduction in velocity (Fig. 7).

The model provides information about the flow regime (i.e. subcritical or supercritical), which is characterized in terms of the Froude number, F_R

$$F_R = \frac{V}{\sqrt{gy}} \tag{3}$$

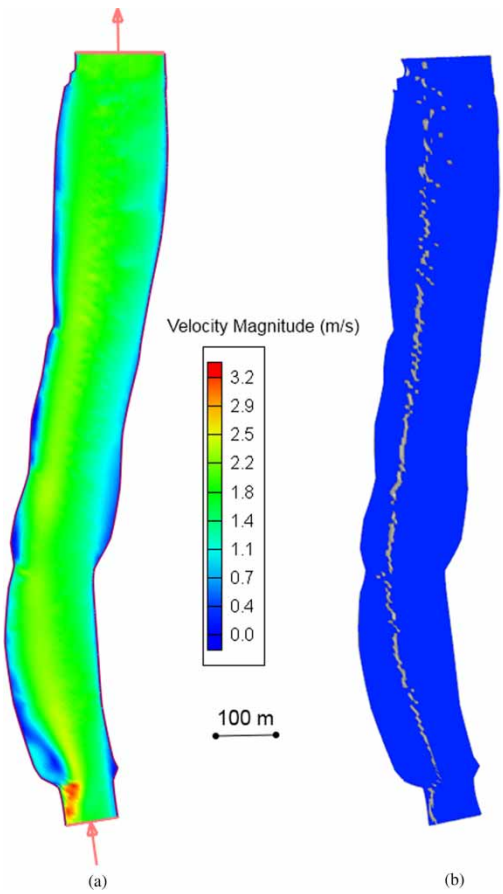

Fig. 9 (a) Velocity distribution and (b) maximum velocities at each river cross-section

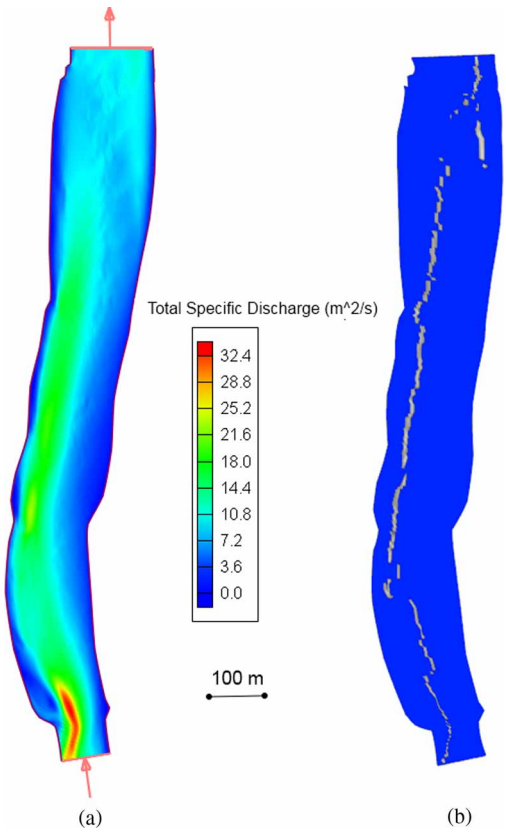

Fig. 10 (a) Specific discharge and (b) maximum specific discharge at each river cross-section

where V denotes the averaged velocity magnitude, g denotes gravity, and y denotes the water depth. The knowledge of the flow condition is important, because water waves and bed forms can be in phase or out of phase according to the flow regime, creating favourable or unfavourable conditions for devices installed in the river. For instance, local water depth is not affected by the motion of bed forms in the supercritical flow regime because waves are in phase with bedforms. However, a reduction in local water depth could be expected in subcritical flows when bedforms are moving near the device because waves can be out of phase with bedforms. Thus, devices installed in subcritical flows could have additional constraints (i.e. avoid the possibility of being partially dry during the motion of bedforms, reduction of area for debris, etc.). The Froude number along the study reach shown in Fig. 11 indicates that flow, under the simulated conditions, falls in the lower regime, or subcritical flow (i.e. $F_R < 1$). The average value of F_R along the thalweg is approximately 0.30.

Model velocity and specific discharge values were exported to a spreadsheet to calculate the maximum velocity and maximum specific discharge at each cross-section along the river reach that are of specific interest in determining the location of maximum hydrokinetic power in the river. These maximum values are shown in Figs 9(b) and 10(b), respectively. The results shown in Fig. 10(b) clearly indicate the instability of the river channel, in terms of thalweg location, in the downstream region where the location of maximum specific discharge suddenly shifts next to the right bank.

The instantaneous power density of a parcel of fluid [**19**, **20**] is defined as

$$[P/A]_{\text{water}} = 1/2\rho V^3 \tag{4}$$

where P denotes power, A denotes cross-sectional area, and ρ denotes water density.

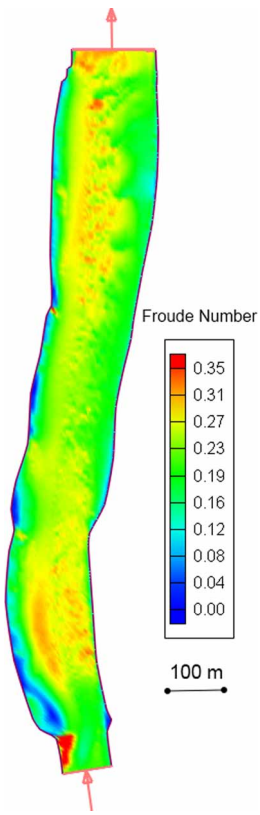

Fig. 11 Froude number along the study reach

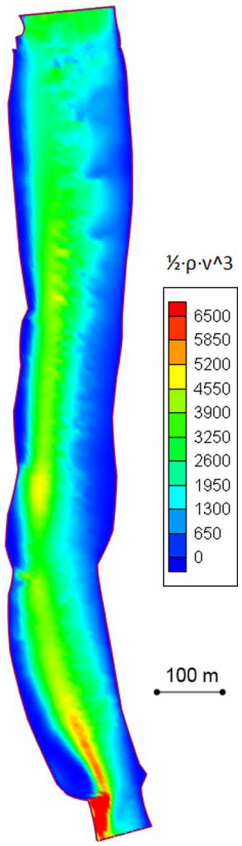

Fig. 12 Instantaneous power density plot

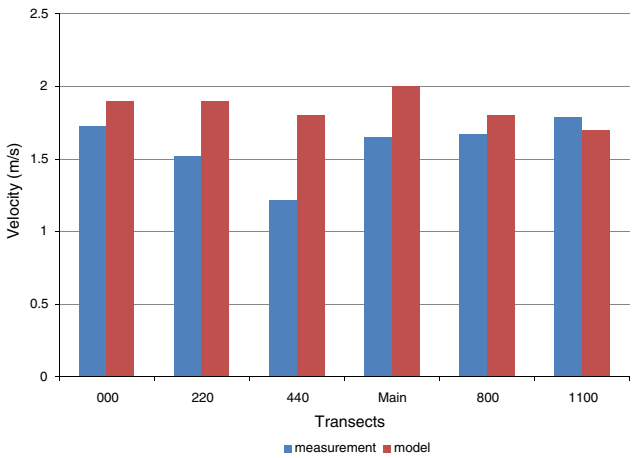

Fig. 13 Comparison between modelled and measured velocities – *thalweg* location

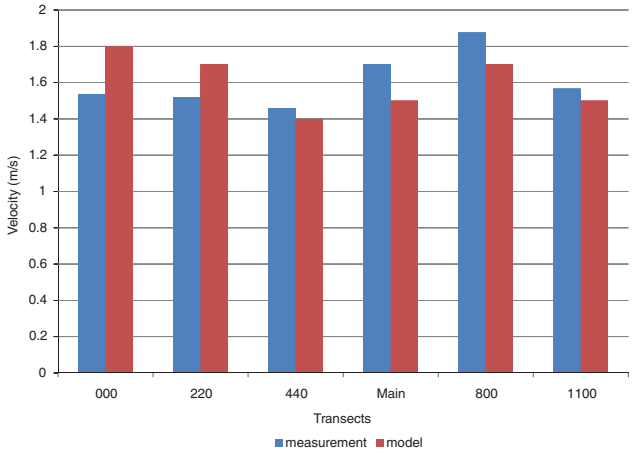

Fig. 14 Comparison between modelled and measured velocities – *maximum* location

Equation (4) was applied to the velocity field produced by the numerical model. The results shown in Fig. 12 indicate the region along the reach where the energy is concentrated. Thus, this plot represents an assessment of the energy available in the Tanana river, at the time of the bathymetric survey. The maximum current velocities specific discharge and highest instantaneous power densities are located in the proximity of the thalweg. Average values in the area of maximum energy are around 4500 W/m^2.

Finally, a comparison between velocity measurements and velocity generated by the numerical model along the thalweg and maximum locations are shown in Figs 13 and 14, respectively. The horizontal axis in both figures indicates the transects where the moored ADCPs were deployed. In general, the model adequately reproduces the velocity measurements. The average difference between modelled and measured velocities is around 3 per cent, which is very good for a 2D model.

5 CONCLUSIONS

A comprehensive methodology to assess the hydrokinetic potential of a reach of the Tanana river near Nenana, Alaska, and provide base-line information to examine the effects of future installed power turbines was developed by characterizing the hydraulic aspects of the reach. The methodology also provides information that can be used to determine the suitability of the reach for installing and operating one or more hydrokinetic electric turbines as part of a planned demonstration by the ORPC.

The methodology mainly focuses on the river discharge, velocity, power density, turbulence, and Froude number. Velocity measurements for extended periods of time in selected locations are used to determine turbulence. A 2D hydrodynamic model is used to extend discrete measurements to define the continuous velocity and specific discharge, and Froude number and their transition conditions throughout the river reach. Model-generated averaged velocity values are used to calculate the instantaneous power density which is the critical component that determines the hydrokinetic potential of the river. Knowledge of bed sediments and detailed bathymetric information is used to build an accurate model bathymetry mesh and estimate realistic bed friction coefficients.

Maximum cross-sectional velocity, specific discharge, and turbulence provided insights about the thalweg condition (i.e. stable versus unstable). For the study site, maximum velocity, maximum specific discharge, and turbulence were localized along the thalweg in the upstream portion of the reach (from transect 000 to about transect 800). Downstream from transect 800 to the end of the reach at transect 1100 the maximum velocity correlated with the thalweg (near the left bank) while the maximum specific discharge and turbulence shifted towards the right bank. These conditions indicate that the thalweg upstream from transect 800 is probably stable while the section of thalweg downstream from transect 800 may be shifting towards the right bank.

The Froude number indicates that the flow is subcritical in the river reach with an average value of 0.30 along the thalweg. This situation could be problematic when deciding the location of devices in the river, as the waves and bedforms can be out of phase.

The averaged transect-measured velocities along the thalweg are about 1.5 m/s with maximum values of around 1.9 m/s. Model-calculated maximum velocities along the thalweg are about 3.6 m/s at the upstream end of the reach and between about 1.5–2 m/s along the remainder of the thalweg. The average value for instantaneous power density is approximately 4500 W/m^2, for the simulated river settings, at the period of measurement (i.e. late August) with a maximum of about 6500 W/m^2 at the upstream part of the reach.

Scaled profiles of velocity as a function of distance from the riverbed in the thalweg indicate that current velocities increase to their maximum values within about 60 per cent of the distance from the riverbed to the surface and remain relatively constant to the surface. Exceptions to this general observation occur for transects 440 and 1100 where current velocities decrease as the distance from the riverbed increase (near the river surface) after passing through a maximum value, which may indicate chaotic or back eddy flow at these locations. Local bathymetry could modify the development of boundary layers in these cross-sections.

The reach of Tanana river examined in this study appears to have a stable thalweg that carries the maximum velocity, discharge, and instantaneous power density, with sufficient magnitudes to drive a hydrokinetic turbine, from transect 000 to about

transect 800. The flow regime in the entire reach is subcritical. The vertical velocity profiles indicate that current velocities generally increase from the riverbed to the surface reaching maximum values at about 0.6 of the river depth above the riverbed for all transects above 800 except for transect 440. With the exception of the region around transect 440, these conditions may be suitable for a hydrokinetic turbine. The river reach below transect 800 appears to be unstable and may pose challenges to an installed turbine.

ACKNOWLEDGEMENT

Data used in this work were obtained from the project supported by the Alaska Energy Authority, contract 2195437/G00005572.

REFERENCES

1 **Miller, G., Franceschi, J., Lese, W.,** and **Rico, J.** The allocation of kinetic hydro energy conversion systems (KHECS) in USA drainage basins: regional resource and pontential power. Final report, NYUDAS 86-151, August 1986, p. 54.

2 AEA. Alaska renewable energy and energy efficiency development short to mid-term objectives. Anchorage, Alaska Energy Authority, 2007, p. 3, available from http://www.climatechange.alaska.gov/docs/sc3_AEA.pdf.

3 **Previsic, M.** and **Bedard, R.** River in-stream energy conversion (RISEC) characterization of Alaska sites, 29 February 2008, EPRI PP-003-AK, April 2006.

4 **Previsic, M., Bedard, R.,** and **Polagye, B.** System level design, performance, cost and economic assessment – Alaska river in-stream power plants, EPRI RP-003-AK, 31 October 2008.

5 **Wilson, M., Saylor, B., Szymoniak, N., Colt, S.,** and **Fay, G.** Components of delivered fuel prices in Alaska, 2008. Prepared for the Alaska energy authority. Anchorage: University of Alaska Anchorage Institute of Social and Economic Research, 2008.

6 AEA/ACEP (Alaska Energy Authority and Alaska Center for Energy and Power). Alaska energy: a first step toward energy independence, 2009, p. 245, available from http://www.aidea.org/AEA/PDF%20files/AK%20Energy%20Final.pdf.

7 **Muste, M., Yu, K., Pratt, T.,** and **Abraham, D.** Practical aspects of ADCP data use for quantification of mean river flow characteristics; Part II: fixed-vessel measurements. *Flow Meas. Instrum.*, 2004, **15**, 17–24.

8 **Tennekes, U.** and **Lumley, J.** *A first course in turbulence*, 1972 (MIT Press, Cambridge, MA).

9 **Tevez, A., Mattar, M., Toniolo, H., Fernandez, R.,** and **Lopez, F.** Mean flow and turbulence structure over dunes with superimposed smaller bedforms. In Proceedings of the 28th IAHR Congress, Graz, 1999.

10 **Snedecor, G.** and **Cochran, W.** *Statistical methods*, 8th edition, 1989 (Iowa State University Press, Ames, Iowa, USA).

11 **Kleinbaum, D.** and **Kupper, L.** *Applied regression analysis and other multivariable methods*, 3rd edition, 1997 (Duxbury Press, Pacific Grove, California, USA).

12 **Jia, Y., Scott, S., Xu, Y.,** and **Wang, S.** Numerical study of flow affected by bendway weirs in Victoria Bendway, the Mississippi River. ASCE *J. Hydraul. Eng.*, 2009, **135**(11), 902–916.

13 **Zhang, Y.** CCHE-GUI – Graphical Users Interface for NCCHE Model User's Manual – Version 3.0, Technical report no. NCCHE-TR-2006-2, National Center for Computational Hydroscience and Engineering, October 2006.

14 **Jia, Y.** and **Wang, S.** CCHE2D Verification and Validation Tests Documentation, Technical report no. NCCHE-TR-2001-2, National Center for Computational Hydroscience and Engineering, August 2001.

15 **Jia, Y., Wang, S.,** and **Xu, Y.** Validation and application of a 2D model to channels with complex geometry. *Int. J. Comput. Engng Sci.*, 2002, **3**, 57–71.

16 **Crowe, C., Elger, D., Williams, B.,** and **Roberson, J.** *Engineering fluid mechanics,* 9th edition, 2009 (John Wiley & Sons, Hoboken, New Jersey, USA).

17 **Afzalimehr, H.** and **Dey, S.** Influence of bank vegetation and gravel bed on velocity and Reynolds stress distributions. *Int. J. Sediment Res.*, 2009, **24**(2), 236–246.

18 **Garcia, M.** Hydraulic jumps in sediment-driven bottom currents. *J. Hydraul. Eng.*, 1993, **119**(10), 1094–1117.

19 **Bryden, I., Couch, S., Owen, A.,** and **Melville, G.** Tidal current resource assessment. *Proc. IMechE, Part A: J. Power and Energy*, 2007, **221**, 125–135. DOI: 10.1243/09576509JPE238.

20 **Polagye, B., Kawase, M.,** and **Malte, P.** In-stream tidal energy potential of Puget sound, Washington. *Proc. IMechE, Part A: J. Power and Energy*, 2009, **223**, 571–587. DOI: 10.1243/09576509JPE748.

APPENDIX

Notation

A	cross-sectional area
F_R	Froude number
g	gravity
i	direction in co-ordinate system; $i = 1$ = east, $i = 2$ = north, $i = 3$ = vertical upward
P	power
Q	water discharge
R_{ij}	Reynolds stress tensor
u	velocity fluctuation
$\tilde{u}$	instantaneous velocity
$\overline{u_i^2}$	average of the square of the normal velocity fluctuations
$\overline{u_1 u_2}$, $\overline{u_1 u_3}$, $\overline{u_2 u_3}$	average of the products of velocity fluctuations in two (shear) directions
U	mean flow velocity
V	velocity magnitude
y	water depth
ρ	density of water